Solid Freeform Fabrication Using Semi-Solid Processing

by

Christopher S. Rice

B.S., Mechanical Engineering, 1993
University of Colorado, Boulder

Submitted to the Department of Materials Science and Engineering in Partial Fulfillment of the Requirements for the Degree of Master of Science

at the

Massachusetts Institute of Technology
June 1995

Signature of Author .....
Department of Materials Science and Engineering
May 12, 1995

Certified by .....
Stuart B. Brown
Richard P. Simmons Associate Professor of Materials Manufacturing
Thesis Advisor

Accepted by .....
Carl V. Thompson II
Professor of Electronic Materials
Chair, Departmental Committee on Graduate Students

Solid Freeform Fabrication Using Semi-Solid Processing

by

Christopher S. Rice

Submitted to the Department of Materials Science and Engineering on May 12, 1995 in Partial Fulfillment of the Requirements for the Degree of Master of Science in Materials Science and Engineering

Abstract

A proof-of-concept prototype has been developed to demonstrate the feasibility of solid freeform fabrication using semi-solid metals. A model system of 85% Sn-15% Pb slurry was used to generate 3-dimensional components in a freeform fabrication process. These components are near net shape and possess advantages over other methods of manufacture. The components are metal, fully dense, and produced quickly. Immediate application in rapid prototyping is evidenced, as well as potential for cost-effective small-scale flexible manufacturing.

Thesis Supervisor: Stuart B. Brown
Title: Formerly Richard P. Simmons Associate Professor of Materials Manufacturing

Table of Contents

List of Figures

Acknowledgments

The author would like to extend a sincere thanks to Stuart Brown, whose ideas, insight, and encouragement have not only made this project possible but also extremely enjoyable. The author also wishes to thank Professor Brown's research group—Mayank Bulsara, Pratyush Kumar, Patricio Mendez, Will Van Arsdell, and John Wlassich—for their constant stream of input. A final thanks goes to Shinya Myojin for all his efforts in the laboratory and the essential extra set of hands he provided. This work was funded by a Faculty Development Grant from the Leaders for Manufacturing Program at the Massachusetts Institute of Technology.

1.0 Introduction

In recent years, great strides have been made in the advancement of rapid prototyping and flexible manufacturing technology. However, one major need which has remained unsatisfied is a process which can produce structural, fully dense, *metallic* components. In rapid prototyping, it is useful not only to generate components which physically resemble the actual production component, but also to create components which will behave mechanically similar to the real component. And, in the case of flexible manufacturing, it is *required* that the component produced satisfies functional demands. It is clear, then, that a process which can quickly produce metal structural components would be invaluable.

A number of solid freeform fabrication processes now exist which can produce components with good dimensional accuracy. However, they each have limitations, and a few representative processes are briefly discussed here: fused deposition modeling, stereolithography, 3D printing, selective laser sintering, and droplet deposition.

Fused deposition modeling (FDM) involves the deposition of a polymer stream layer by layer on a substrate. Although FDM creates good plastic-based models, the process is limited to certain polymers and wax, and the models therefore lack the strength afforded by metals. FDM is inexpensive to implement, however, and offers the ability to deposit large quantities of thermoplastic relatively quickly.

Stereolithography is a popular process which produces components by selectively and slowly polymerizing layers in a liquid bath. Fabrication of a polymer prototype can require hours of processing. Like fused deposition modeling it is limited to certain polymer compositions (in the case of stereolithography, photo-sensitive polymers) and must be accompanied by a second curing phase after the initial build. 3D Systems, the leading stereolithography company, nevertheless has been successful given the absence of any competing process offering comparable accuracy.

3D printing is capable of producing intricate parts by depositing successive layers of binder on ceramic powder. It has been shown that these parts can possess some degree of strength [1]; however, components produced by 3D printing require firing to cure the green body, and still do not become fully dense.

Selective laser sintering (SLS), which produces metal components by using a laser to sinter layers of metal powder with or without an intermediate binder [2,3], can only yield fully dense components if a subsequent post process such as hot isostatic pressing (HIPing), firing, or infiltration is used. Post-processing of this manner introduces complicated dimensional changes and additional costs which must then be accounted for in the original fabrication. SLS therefore can be used to produce only a small number of metal components where strength is not important, because as with 3D printing the residual porosity so dramatically reduces component strength.

Finally, droplet deposition can also produce metal components. Parts are built by spraying a fine stream of molten metal droplets on successive layers. While able to make small parts with good tolerance, this process is impractical for large components requiring bulk metal because of limited deposition rates. The process suffers from the inherent limitation that its success requires small droplets, and thus low deposition rates. It should also be recognized that each of these processes are slow and have limitations of component size. For a more detailed comparison of commercial SFF processes, the reader is referred to the paper by Aubin [4].

1.1 Solid Freeform Fabrication Using Semi-Solid Metals

The process presented in this paper addresses many of the issues mentioned above. Briefly, solid freeform fabrication uses semi-solid metals to deposit a stream of partially solidified metal alloy slurry on a substrate which moves relative to the slurry. Components are built by depositing the slurry stream in successive layers on one another. At the completion of each layer, the substrate is lowered, and the next layer is deposited. Subsequent layers of the slurry are able to form metallurgical bonds with the previous layers.

This capability is particularly exciting. Unlike the other technologies described in the preceding section, the technology described in greater detail in the following chapters permits the DIRECT, RAPID FABRICATION OF FULLY DENSE, METAL STRUCTURES. We know of no other process that offers these advantages.

1.2 Semi-Solid Metal Processing

To understand this solid freeform fabrication process, it is helpful to discuss briefly the fundamentals of semi-solid metal processing.† The equilibrium phase diagrams of metal alloys show regions of temperature and composition where a liquid phase and solid phase can coexist. Figure 1 is a simple binary phase diagram, and the shaded areas highlight these regions. During the solidification of castings in this partially solidified state, the formation and growth of dendrites is common, whether columnar or equiaxed. As the solid fraction increases past a characteristic value during cooling, the deformation resistance of the partially solidified metal increases dramatically [5]. However, if this same alloy composition is sheared sufficiently during cooling to break up dendrites and form spheroidal solid-phase particles, the deformation resistance is drastically reduced. This combination of solid phase particles suspended in a molten liquid phase is referred to as a semi-solid slurry. Flemings illustrates that a semi-solid slurry created in this manner, specifically an 85% Sn-15% Pb slurry, exhibits a shear strength three orders of magnitude lower than a dendritic system of equal solid fraction [5]. Similar results have been obtained for a large number of engineering alloys [ibid]. Thus, it is possible for slurries of significantly high solid fraction to flow easily.

Semi-solid slurries offer some unique properties which can be exploited in solid freeform fabrication. The flow properties of a slurry stream can be greatly modified by controlling the solid fraction present in the stream. Deformation resistance, or apparent viscosity, can be changed by many orders of magnitude between solid fraction values of 0.1 and 0.9. This effect can be visualized as the difference between the flow of water and

†. The behavior of certain semi-solid slurry systems has been studied extensively [6-16]. For a comprehensive overview of the fundamentals, the reader is referred to papers by Flemings [5] and Brown [12].

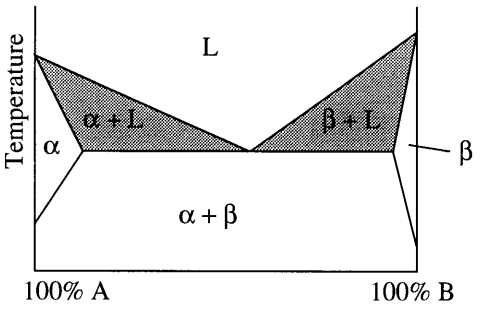

FIGURE 1: Sample binary phase diagram.

the deformation resistance of toothpaste. One can imagine that the deposition of a stream of toothpaste with an apparent viscosity on the order of 100 Pa-sec is more easily controlled than a stream of water. Similarly, use of a metal slurry allows deposition rates unattainable with a fully molten metal. And, as compared to a fully liquid state, semi-solid slurries will undergo less shrinkage during final solidification since much of the slurry is already solid and since the temperature is lower.

1.3 Advantages of Solid Freeform Fabrication Using Semi-Solid Metal Slurries

Before beginning the description of the actual process, we list the advantages of the technology. First, the components that are produced are fully dense metal components. They can therefore be used in structural applications where conventionally cast or machined parts would have been used. Second, the process is well-suited to large parts which require filled bulk regions because it is capable of high flow rates. The only limitation to deposition flow rate is the ability to provide semi-solid to the substrate. Third, by controlling the solid fraction and shear history of the slurry, one can control the microstructure of the metal component. This control would allow for components which possess differing material properties in different areas. And finally, once the part has been formed during deposition, no de-binding, curing, HIPing, or infiltration is required to create a structural component.

2.0 Process Description

Three major iterations of design occurred during the course of this research. The machines that were designed will be referred to as Generations I, II, and III indicating the order in which they were implemented, with Generation I being the first. Generations I and II were similar in that they were each a "pseudo-continuous" process where a molten source of liquid is slowly cooled into the semi-solid state as it is stirred and flows through the length of the machine. Generation III, on the other hand, is a batch process in which a non-replenishable source of material is melted, cooled and stirred in place, and then ejected out of the machine. This section details the design of each machine and discusses the associated experimental procedures.

2.1 Generation I

Figure 2 is a schematic of the Generation I rheocaster used for producing a stream of semi-solid slurry. The rheocaster consisted of two main sections—an upper reservoir and a lower mixing chamber. The reservoir was made from 4 inch diameter 1024 steel tubing and heated by one large 850W band-type resistance heater. Its function was to contain a fully liquid alloy bath, which flowed to the lower chamber. The lower chamber, also 1024 steel tubing, was equipped with several resistance heaters along its 6 inch length as shown. Several K-type thermocouples were inserted into blind holes along the length of the tube to allow for temperature measurement and control. All temperature measurements were acquired by a Kiethley Model 5000 data acquisition module sampling at 1 Hz attached to a 386 personal computer and processed by Labtech Notebook software. The tubing was insulated on the outside with 1-inch-thick alumina silica ceramic fiber blanket. As the molten alloy flowed from the reservoir through the length of the chamber, it was cooled to a partially solidified state and sheared by a turning rotor. The rotor was machined from 304 stainless steel tubing, and extended the entire length of the apparatus. The bottom end of the rotor was closed with a solid tapered stainless steel fitting to match the geometry of the exit nozzle. The rotor was driven by a Siemens model 1FT-5064 servo

motor with a Simodrive 610 controller. Rotor speed was controlled through Labtech Notebook, and torque measurements from the servomotor were monitored to avoid overloading the motor. At the bottom of the mixing chamber was a conical nozzle. The nozzle had a taper of 45° and an exit diameter of 9/64 inch. This diameter was found to be the smallest through which the semi-solid would flow continuously.

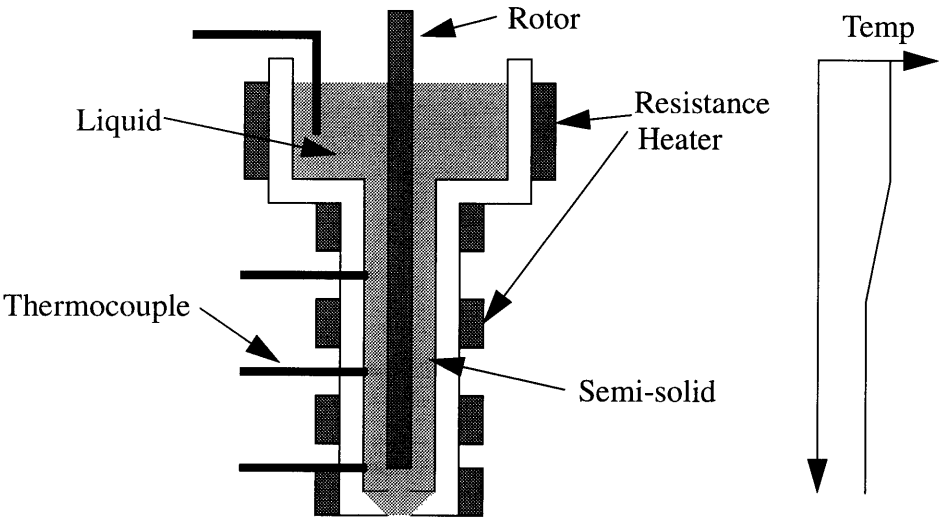

FIGURE 2: Schematic of Generation I machine.

Typical experiments consisted of the following steps: The reservoir was loaded with approximately 1 kg of small pieces of 85% Sn-15% Pb alloy (about 1/2 in. x 1/4 in. x 1/2 in.), and the bottom of the mixing chamber was plugged. The reservoir and chamber were then both heated to 211 °C (slightly above the liquidus of 209°C [6]). Once the entire system was superheated, the rotor was started and set to the desired rotation rate. Typically, that value was 70 rpm. Soon after starting the stirring, cooling of the lower chamber commenced by natural convection while the reservoir temperature remained above the liquidus. We found that a decreasing gradient from the top of the chamber to the middle, followed by a constant-temperature regime, provided best results. The constant temperature regime was usually controlled to be near 190°C. The approximate desired temperature profile is shown in the right of figure 2. Figure 3 shows the measured temperature profile for a given experiment. Temperature is plotted as a function of distance from the orifice.

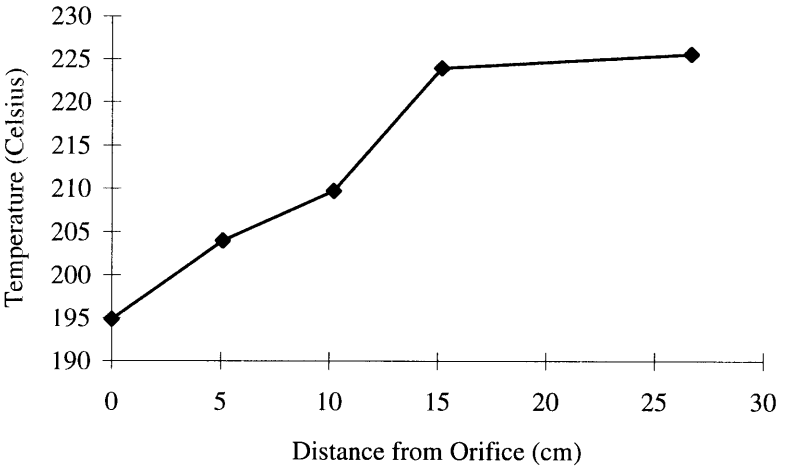

FIGURE 3: Representative temperature profile of Generation I machine.

When the desired temperature profile was achieved, the plug was removed to allow the flow of semi-solid. The first few seconds of flow were usually liquid—which we believe to be a result of floatation of the Sn-rich solid phase—followed by a transition to a steady state semi-solid flow.

Although the Generation I machine was able to produce a continuous stream of semi-solid slurry and prove the feasibility of the design during the twenty experiments which were run with it, it suffered from several limitations. First, it left the molten reservoir open to atmosphere, allowing for oxidation on the surface of the molten metal, and subsequent entrapment of impurities. Second, we found it desirable to have a larger capacity for material in the system. And finally, the machine relied on natural convective cooling of the mixing chamber; while it was possible to obtain repeatable temperature profiles for the chamber, the cycle time for cooling was slow (on the order of 30 minutes), and we were limited in the types of profiles we could achieve. Appendix I shows two representative temperature history profiles. Generation II addressed each of these issues.

2.2 Generation II

Figure 4 is a schematic of the Generation II rheocaster. The rheocaster's basic design and function was similar to that of Generation I. It, too, consisted of two main

sections—an upper reservoir and a lower mixing chamber. The reservoir was made from 304 stainless steel tubing (to avoid rusting of the exterior experienced in Generation I experiments) and heated by one large band-type resistance heater. In this generation, a stainless steel plate with an argon intake valve was sealed to the top of the chamber to allow for an inert atmosphere. The lower chamber, extended to 10 inches to accommodate more semi-solid material, was also 304 stainless tubing equipped with alternating resistance heaters and air cooling coils along its length as shown. These coils were added to more precisely control temperature during cooling. Numerous K-type thermocouples inserted through the tubing into the slurry along the length of the chamber allowed precise temperature measurement and provided feedback for PID control of the heating elements. To reiterate, the changes incorporated the following in Generation II:

- copper air-cooling tubes on the mixing chamber
- thermocouple holes which fed through to the semi-solid slurry
- stainless steel components
- longer mixing chamber and rotor
- inert gas environment.

As in Generation I, the molten alloy flowed from the reservoir through the length of the chamber and cooled to a partially solidified state while sheared by an extended rotor.

Experimental procedure was similar to that of Generation I: The reservoir was loaded with approximately 1.5 kg of small pieces of 85% Sn-15% Pb alloy (about 1/2 in. x 1/4 in. x 1/2 in.), and the bottom of the mixing chamber was plugged. The reservoir and chamber were then both heated to 211 °C while argon was flushed through the reservoir. As before, once the entire system was superheated, the rotor was started and set to the desired 70 rpm. Soon after starting the stirring, cooling of the lower chamber commenced while the reservoir temperature remained above the liquidus. By flowing air through the cooling tubes and lowering the power output of the heaters, any number of possible temperature profiles could be generated in the mixing chamber. We found that a decreasing gradient from the top of the chamber to the middle, followed by a constant-temperature regime, provided best results. The constant temperature regime was usually

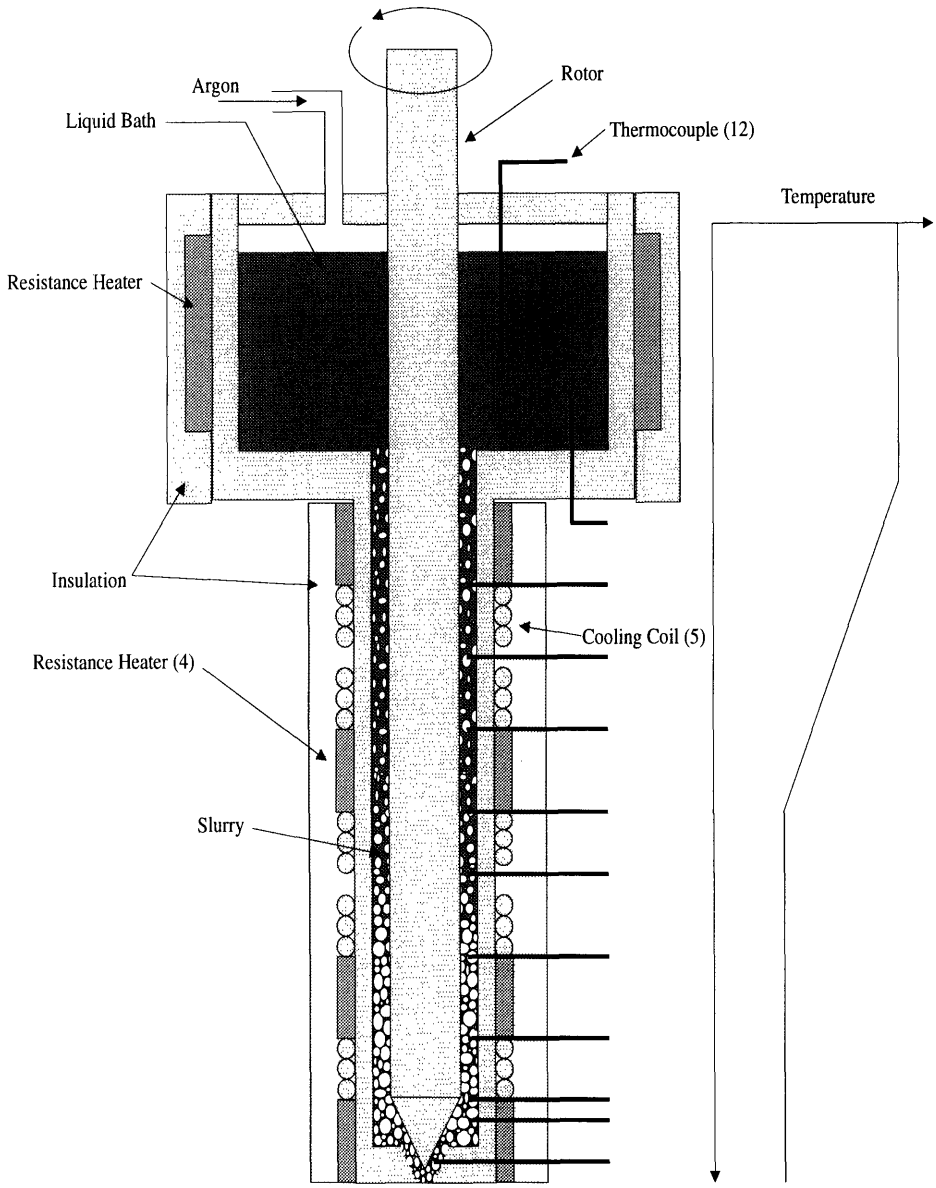

FIGURE 4: Schematic of Generation II continuous rheocaster.

controlled to be at or around 190°C. The approximate temperature profile is shown in the right of figure 4. Figure 5 illustrates the precise temperature profile obtained during an experiment. Four profiles are shown, one at each of four different moments in time. One can observe the evolution of the temperature profile to one much like that which is desired. Approximately 50 experiments were performed with Generation II.

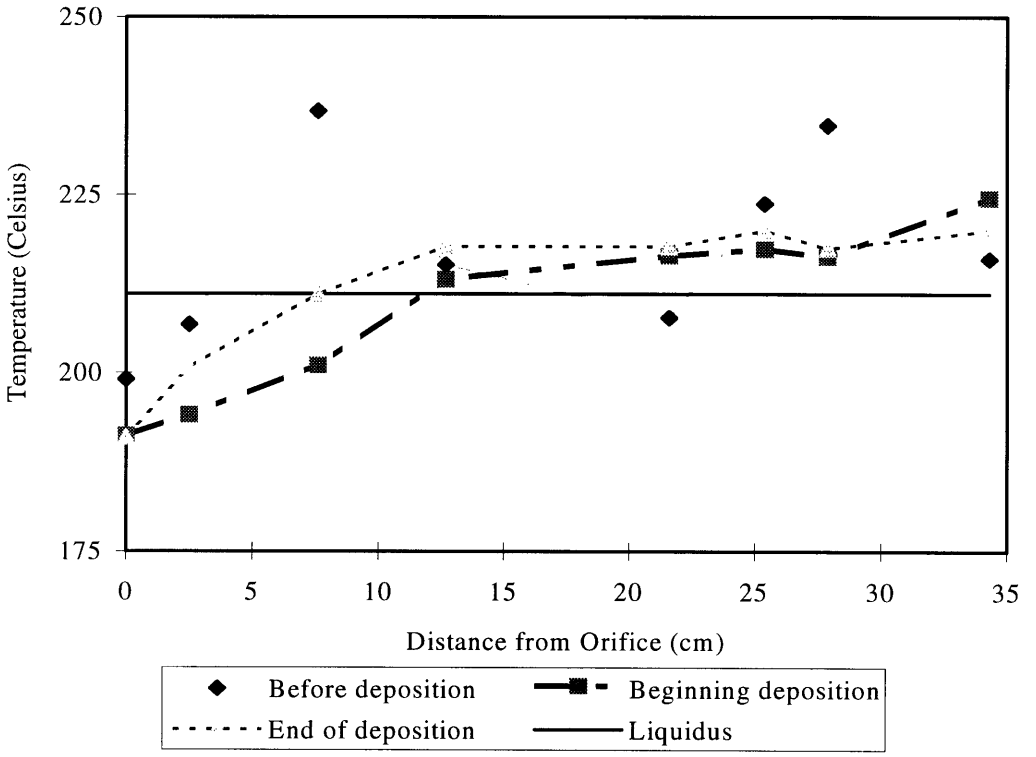

FIGURE 5: Representative temperature profile for Generation II.

Again, upon achieving the desired temperature profile, we removed the plug to allow the flow of semi-solid. The first material to exit was liquid followed by a transition to semi-solid flow. This semi-solid stream could then be deposited on a moving substrate. The substrate motion was controlled by a 3-degrees-of-freedom translating table. The table was driven by three Daedal MS Series stepper motors controlled by a Compumotor AT6400 Indexer and could be programmed to follow most desired 3-dimensional paths. The paths were generated by manually sectioning 3D AutoCad files and fitting contours to the resulting sections. The task was fairly arduous given the need to translate component geometries to deposition paths. Paths were then programmed manually on a 80486

personal computer in a commercial programming language similar to BASIC. These paths were downloaded to the AT6400 and precompiled before execution. All 3-dimensional geometries were created using this programmable x-y-z table. Figure 6 is a schematic showing the system layout. Appendix IV provides representative programs used to control the motion of the x-y-z table.

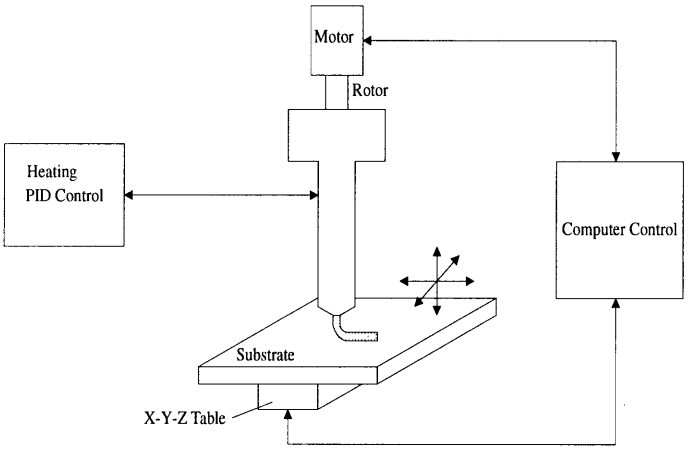

FIGURE 6: Schematic of deposition system.

Figure 7 is a photograph of two components manufactured using metal solid freeform fabrication (MSFF), from the Generation II machine. The component at the left of figure 7 is a pipe section which increases and then decreases in diameter from top to bottom. It is 82 mm high. The component at right is a pipe bend section. Each would be difficult to cast or otherwise form. They each required approximately one minute of deposition with the mentioned process. SFF technologies such as 3D printing or selective laser sintering would require hours to manufacture these geometries, and the components would be porous. It should be noted that the surface finish of components like those shown in figure 7 is not as smooth as that found with other SFF processes. These components have been produced with little attention paid to surface finish, as the goal of this research was to prove the layering concept with semi-solids. Surface finish is of great interest in industry and will certainly be a focus of future efforts. Figure 8 shows a commercial, mass produced pipe elbow (left) and a MSFF elbow for comparison. A plug has been threaded into the MSFF elbow to illustrate the capability of finish machining.

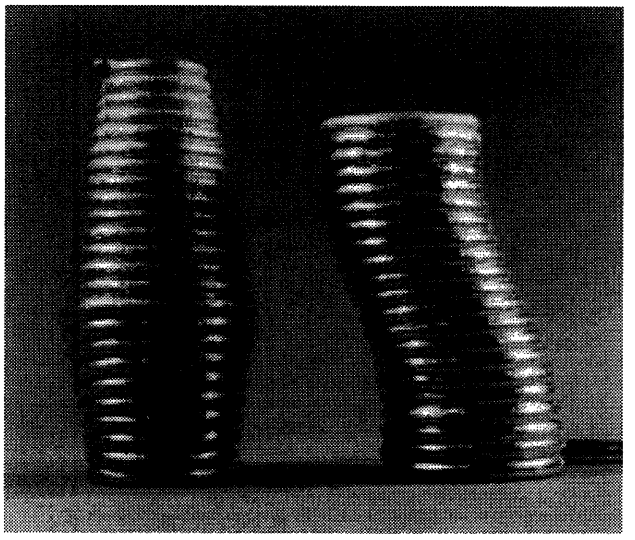

FIGURE 7: Sample MSFF components.

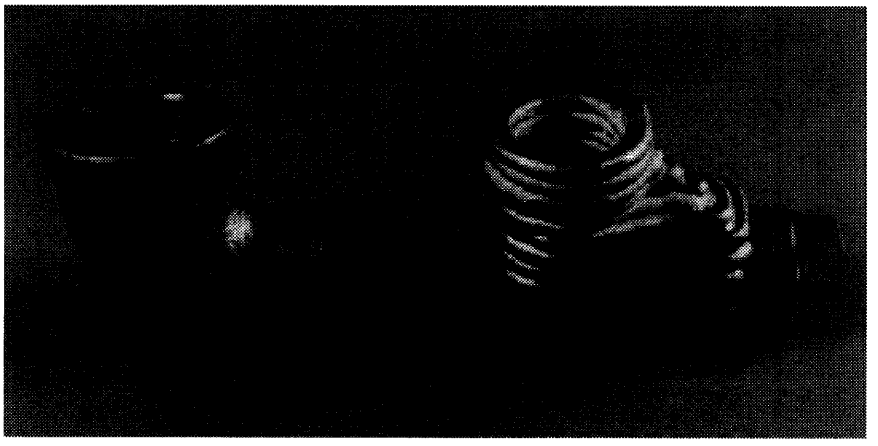

FIGURE 8: Pipe elbows of conventional (left) and MSFF manufacturing.

An important consideration for this model system was the alloy selection. An 85% Sn-15% Pb system was chosen because it is a low-temperature system and one which has been studied in detail [6-9, 11]. The 85% Sn-15% Pb system allows the use of stainless steel components in processing, and data exist for solid fraction vs. temperature [6]. In addition, this system has a relatively large freezing range value in which to process. The alloy therefore provided a suitable composition for the first implementation of this technology. Basic requirements of the system were that:

- it be a continuous system,

- it supply a sufficient shearing history to provide an appropriate microstructure to the semi-solid,
- it accurately measure and control the temperature history throughout the process,
- it allow for a variety of drive methods should the need arise.

With the exception that the systems were not fully continuous, the machines satisfied the above requirements. Sufficient shearing was supplied by the rotor to completely break up any dendritic growth and form rounded solid phase particles with typical maximum dimensions of 80-100 microns. Figure 9 is a micrograph of slurry created by this system and will be discussed in more detail later. Several rotor modifications were made in an attempt to improve the flow control of the system in Generation II; however, this area needs more exploration.

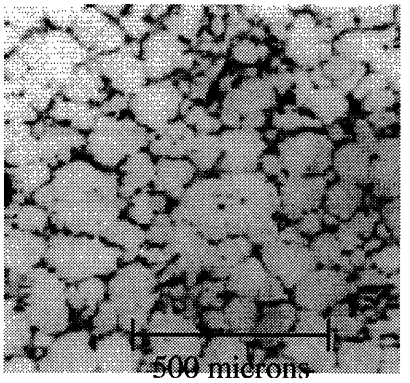

FIGURE 9: Micrograph semi-solid slurry from Generation II.

In the case of the Generation II design, important system variables were monitored or controlled. Measurable quantities included temperature and motor torque. All temperature and torque measurements were continuously monitored and recorded on a 80386 personal computer using the commercial data acquisition software Labtech Notebook. Temperature monitoring was key to the success of our project, and we were successful in reproducing a given temperature profile for many different experimental trials. Torque measurements indicated whether solid fraction was relatively high or low, and would signal the onset of freezing within the system so that it could be avoided.

The system was made versatile by allowing several variables to be controlled directly. Those variables were heating rate, cooling rate, rotor speed, and rotor clearance. Once we found a rotor speed (shear rate) which produced an appropriate slurry, we were able to control attributes such as solid fraction by using the alternating heaters and cooling coils. Rotor clearance with the nozzle was found to affect the flow rate and could be adjusted accordingly by raising or lowering the rotor.

2.3 Generation III

Generation II produced consistent, repeatable streams of semi-solid. However, the flow rate was a function of temperature, shear rate, and height of remaining material left in the system. It was thought that ideally the flow rate should be decoupled from these variables. One such solution is to control the flow of material with the use of a piston, thereby using displacement control. Generation III was designed to force a batch of semi-solid material out of a shot sleeve to create the desired slurry stream. A schematic of this apparatus is shown in figure 10. In this design, a shot sleeve was machined out of 304 stainless steel stock. It measured 5 inches long by 2.5 inches in inner diameter. At the bottom of the sleeve was a removable bottom which could be changed to experiment with exit orifice size. The shot sleeve was heated with a mica-type band heater and mounted in an axial bearing as shown to accommodate slight misalignment with the piston. The piston was also 304 stainless steel, with a removable piston head. The piston was attached to a 20,000 lb tension/compression load cell which was in turn mounted to a 10,000 lb dual screw Instron testing machine. The piston was heated with a flexible "wrap-type" resistance heater. Temperatures were measured on the piston and in the shot sleeve, and recorded in Labtech Notebook on a 80386 personal computer. Load measurements were also recorded by the computer.

In these experiments, the shot sleeve was loaded with 1/2 inch x 1/4 inch x 5 inch bars of 85% Sn-15% Pb and heated so that the bars would melt. Once molten, the metal was cooled while stirred with a removable rotor. Once a desired fraction of the material solidified (typically 30%-40%, indicated by temperature), the rotor was removed and the piston was lowered into the sleeve. As the piston was lowered, semi-solid metal was forced out of the orifice.

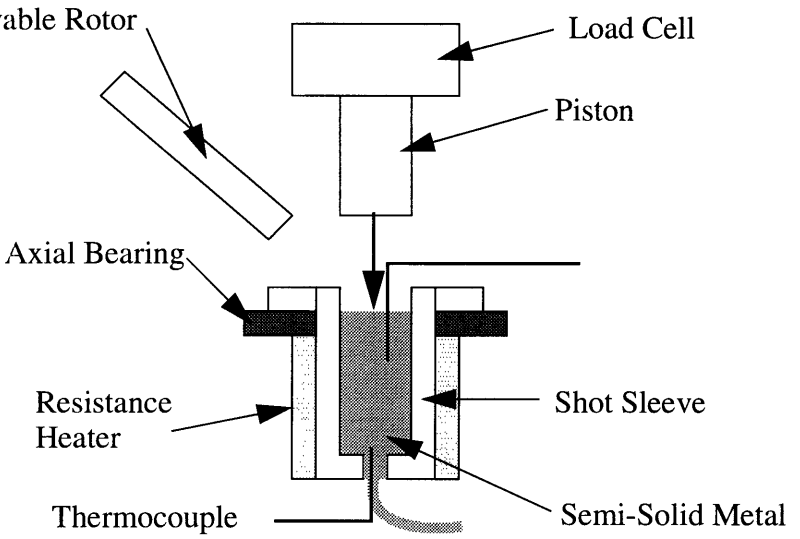

FIGURE 10: Schematic of Generation III machine.

This implementation was not pursued in as much detail as Generations I and II for two reasons. First, once successfully shown to produce tin-lead slurry, it was felt that more attention should be directed to implementing the same design with aluminum semi-solid slurry. There was insufficient time to implement this design in aluminum, however. And second, as is discussed in the following section, the forces required to push the semi-solid from the sleeve reached the limits of the load frame.

3.0 Results and Discussion

Several important characteristics of our process should be noted. These characteristics may define limits to the application of the process, thereby constraining the types of components that may be fabricated.

3.1 Fractionation

First, we believe that during stirring of the semi-solid a separation of phases occurred due to floatation of the relatively lower density Sn-rich solid phase. Initial ejection of fully molten metal from the Generation I and II apparati at temperatures which should correspond to a substantial solid fraction supports this conjecture. Furthermore, densities of components created from 85% Sn stock were measured and found to correspond to tin compositions as high as 95%. To confirm that fractionation was occurring, calorimetry experiments were performed on material samples taken from the slurry stream at various times during the experiments. The samples were reheated until molten and then allowed to cool in air. The temperature of these samples would fall until reaching the liquidus temperature, at which point the temperature would remain constant for tens of seconds. This temperature was recorded for each specimen. From the phase diagram for Sn-Pb, these liquidus temperatures can be translated to composition. Table 1 summarizes these results.

Experimental Time Elapsed (s)	**Liquidus Temperature (°C)**	**%Sn**
0	202	78
30	215	88
60	225	95

TABLE 1: Summary of Calorimetry Results

These data indicate that fractionation did indeed occur in the Generation II machine, as we see a higher concentration of the less-dense Sn-rich composition later in

the experiment. Complete characterization of this separation phenomenon was difficult, and we did not have the time to investigate the factors controlling its onset or extent. Certainly flow separation of liquid and solid phases in a shearing field is well known [18]. The implementation of a stirring mechanism that maintains a homogeneous slurry while imparting sufficient shearing forces and control of the thermal field remains a primary challenge in future generations of this technology.

Other rotor designs, such as helical rotors and stirring techniques such as oscillating, reversing rotation failed to both reduce phase separation and produce a more acceptable slurry in Generation II. This effect did not pose a serious problem, however, because once flow began from the rheocaster an even flow of semi-solid material could be achieved following a brief liquid ejection. The Generation III machine produced slurry which did not vary in composition. We believe that less vigorous stirring in this machine, coupled with a shorter vertical distance over which the slurry flowed, contributed to less floatation and separation of phases.

3.2 Steady State Conditions

The second inherent characteristic of these systems is the steady-state semi-solid flow behavior. In most experiments with Generation II, the flow of material could be maintained for several minutes. The semi-solid typically flowed at 20 mm/s, and the linear motion of the substrate was set to that speed. The stream diameter was between 3 and 4 mm, and this corresponded to volumetric flow rates of approximately 200 mm^3/s.

The flow speed was a function primarily of solid fraction, with low solid fraction corresponding to higher speeds. A certain solid fraction represented a given desired deformation resistance. Too low a solid fraction (less than 0.5) resulted in insufficient deformation resistance and slumping of the deposited layer. Too high a solid fraction (greater than 0.7) resulted in fracturing of the deposited stream as the translating substrate caused the stream to bend and follow different contours. Heaters with more direct coupling between the heat source and the slurries should make it possible to dynamically change the solid fraction, and hence the flow rate, allowing for tailoring of solid fraction to a given flow path as well as quick filling of solid components. The resistance heaters

currently used cannot transmit energy into the slurry sufficiently fast to modify the solid fraction real-time whereas induction heating would offer that advantage.

In the Generation III machine, the flow of semi-solid was somewhat different from that of Generation II. With this system there was no ejection of liquid at the beginning of experiments. The flow moved directly to its steady-state behavior. It was found that for moderate solid fractions (30%-40%) a minimum exit orifice diameter of 0.5 inches was required. For smaller orifice diameters, the loads required to force the semi-solid out of the orifice exceeded the capacity of the machine.

A simple model based on plane strain extrusion was implemented to predict the loads required based on temperature and shear strength of the slurry. A detailed development of this model is presented by Hoffman and Sachs [19]. This model incorporates a rate-independent measure of the deformation resistance of the material, empirical friction parameters and some limited geometric parameters. It provides, however, an analytic estimate of the forces expected during extrusion. Briefly presented, the stress required to force semi-solid through an orifice (excluding friction on the shot sleeve walls) can be estimated as follows:

$$\sigma = \sigma_{xb} + 2m\frac{\sigma_o}{\sqrt{3}}\frac{2}{D_b}$$

where:

$$\sigma_{xb} = -\sigma_o\left(\frac{1+B}{B}\right)\left(1-\frac{D_b^2}{D_a^2}\right)^B$$

and

σ = extrusion pressure

m, f = empirical friction coefficients

σ_o = shear strength of alloy or slurry

D_b = sleeve diameter = 2.25 in

$$B = \frac{f}{\tan\alpha}, f = m = 0.1$$

D_a = orifice diameter = 0.125 in

α = angle of material entry into die = 45 degrees

Kumar [7] gives $\sigma_o = 3x10^6$ Pa for a slurry under similar conditions. This extrusion pressure σ, or back pressure, acts over the projected area of the sleeve. An additional force is contributed by the shear resistance of the material against the walls of the shot sleeve. This shear resistance must be integrated around the cylindrical area of contact within the shot sleeve. If we add these two effects: back pressure and side wall shear resistance, we calculate that the necessary load is approximately 16,000 lbs, well in excess of the machine capacity. Reducing the diameter of the sleeve and the ratio of sleeve diameter to orifice diameter provides loads which are attainable.

Since the speed of the Instron was limited to less than 2 inches per second, we were limited to using a large shot sleeve diameter to achieve higher flow rates of 20 mm/s through a smaller (0.125-0.50 inches) orifice. Unfortunately, at the low solid fractions required to not overload the machine, and the large orifice size, the material did not hold its shape well. We can model how well the semi-solid material will resist deformation, or hold its shape, with a dimensionless group, *Me* [17].

$$Me = \frac{\rho g t L}{9\mu} \qquad \text{(I-1)}$$

where:

ρ = density

g = acceleration of gravity

t = characteristic time

L = characteristic dimension

μ = apparent viscosity

When L is a vertical dimension (in this case the slurry thickness), values of Me much larger than one indicate liquid-like behavior, much smaller than one solid-like behavior, and not far from one typical semi-solids and pastes. We can estimate typical values of Me during deposition. For the semi-solid slurry deposited: $\rho = 7438 \text{kg/m}^3$, $g = 9.81 \text{m/s}^2$, and $L = 0.012 \text{m}$. From temperature data a characteristic time can be estimated as $t \approx 5$ seconds, which is the time associated with solidification of the slurry stream. The following empirical formula fits the data reported by Kumar [7] for globular semi-solid structure between $f_s = 0.30$ to 0.45:

$$\mu = 8.5787 \times 10^{-2} f_l^{-4.642}$$

where:

μ = apparent viscosity in Pascal-seconds

f_l = liquid fraction in kg/kg

For a slurry of f_l=70% we obtain μ=0.45 Pascal-seconds. These values yield $Me \approx 1000$. This number agrees with experiments: the slurry does not flow like a liquid, but deforms easily when deposited on the substrate. Mendez [17] found that for values of Me over 100-200, semi-solid streams tended to slump and not to retain their shape.

3.3 Bond Between Layers

Bonding between layers was found to be very good. Figure 11 shows two representative layers bonded to one another. The solid phase particles appear white while the lead-rich liquid phase appears dark. It is apparent that the microstructure remains constant across the layers. One can see where the layers meet at the left edge, but any sign of an interface through the cross section cannot be found. The rounded, fine grain, solid phase particles lead to more favorable mechanical properties than the dendritic structure typically found in castings. It should be noted that under conditions of high convective cooling rates and high solid fraction, inadequate bonding and delamination did take place.

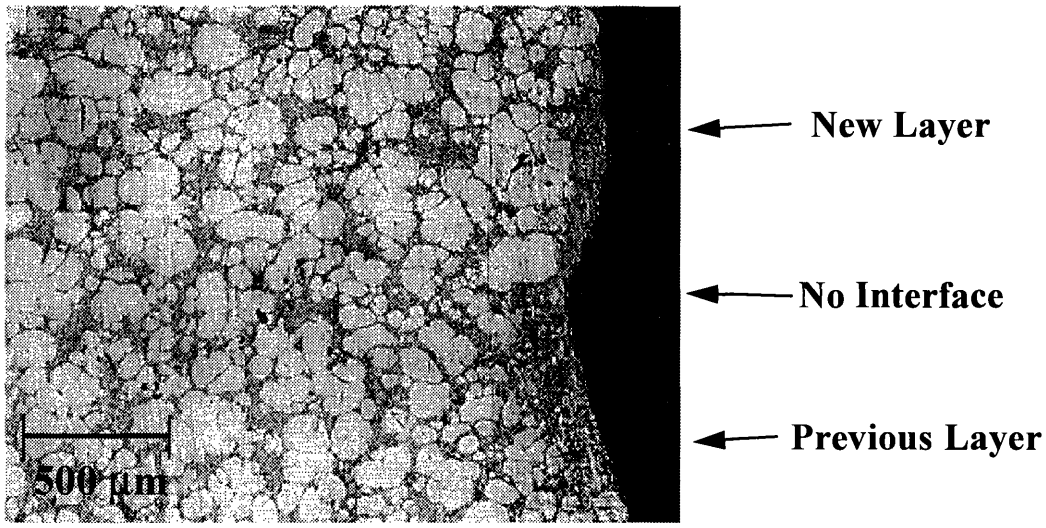

FIGURE 11: Micrograph of two consecutive layers.

Tensile tests were performed on bonded layer structures to assess the mechanical quality of the interface between subsequent layers. Tensile specimens were machined from both cast 85%Sn-15%Pb barstock and semi-solid deposited components. The geometry of the tensile specimens is shown in figure 12. During testing, a displacement-controlled tensile machine was used. The displacement rate was 1 in/min, which corresponds to an equivalent strain rate of approximately 1.9×10^{-2} in/in/s. This high strain rate was selected to reduce rate-dependent effects; room temperature is a high homologous temperature for a Sn-Pb alloy. Table 2 tabulates the results of these tests.

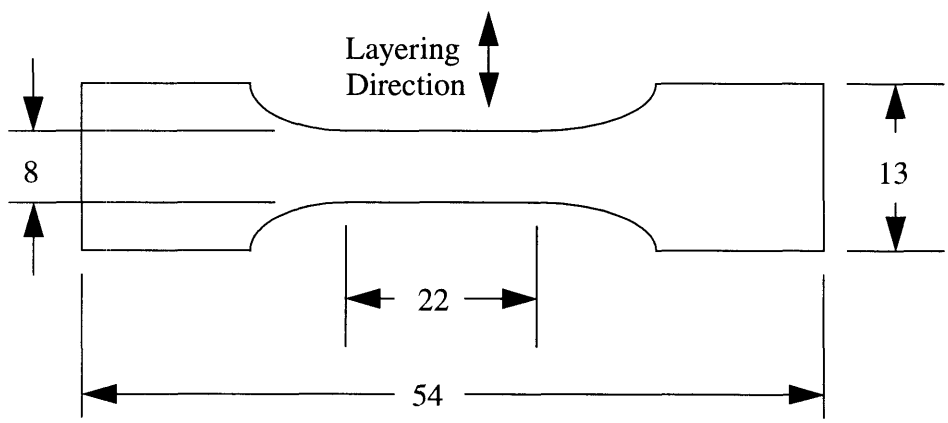

FIGURE 12: Dimensions of tensile specimens (mm).

Test #	UTS	Thickness
	(MPa)	(mm)
1-(bonded)	56.0	4
2-(bonded)	55.4	4
3-(bonded)	54.9	4
4-(bonded)	55.3	5
5-(bonded)	52.9	5
6-(bonded)	48.4	5
7-(cast)	58.5	4
8-(cast)	59.5	5
9-(cast)	49.2	5
Average (bonded)	53.8±4	
Average (cast)	55.7±4	

TABLE 2: Results of Tensile Tests

Tests 1-6 were performed on specimens created by layering semi-solid slurry, while tests 7-8 were performed on raw bulk material. The table shows average values of ultimate tensile strength for both the bonded layer specimens and the barstock specimens. The average UTS for the bonded specimens was 53.8±4 MPa, and the average UTS for the control specimens was 55.7±4 MPa. Within the limits of the error of measurement, these values are indistinguishable, suggesting that the layered components are as strong as the bulk material.

3.4 Overhang of Adjacent Layers

It was found that a maximum angle of free overhang exists during the deposition of layers. Because the orifice cross section was circular, layers tended to "roll" off of one another when the angle became too great. This angle was highly dependent upon the temperature of the slurry exiting the nozzle. An oriented, square or rectangular orifice would help to alleviate this problem. In addition, a greater free overhang can be achieved by reducing the layer thickness, or alternatively by co-depositing layers of powder to act as support for subsequent metal layers. There is no fundamental restriction to co-deposition of powder. It was however beyond the scope of this investigation. In our experiments we have constructed collars for use in regions of large overhang to support

the semi-solid stream. The component pictured in figure 8 employed such support collars for the first two deposited layers of semi-solid.

3.5 Microstructural Characterization

The microstructures obtained using the semi-solid deposition apparatus are representative of semi-solid materials found in the literature, including those by Joly [6]. The solid fraction produced by the apparatus was difficult to determine, as a set of experiments demonstrated. Figures 9 and 11 present the microstructures from deposited components that were allowed to air cool. Figure 13 presents the same composition where the semi-solid stream was directed into an ice-water bath, quenching the slurry. Notice the dramatic difference in apparent solid fractions. The process of solidification in the case of the deposited slurry apparently permits growth of the particle interfaces into the liquid matrix. The microstructures of the fabricated components therefore may suggest a higher solid fraction that actually existed at the moment of deposition.

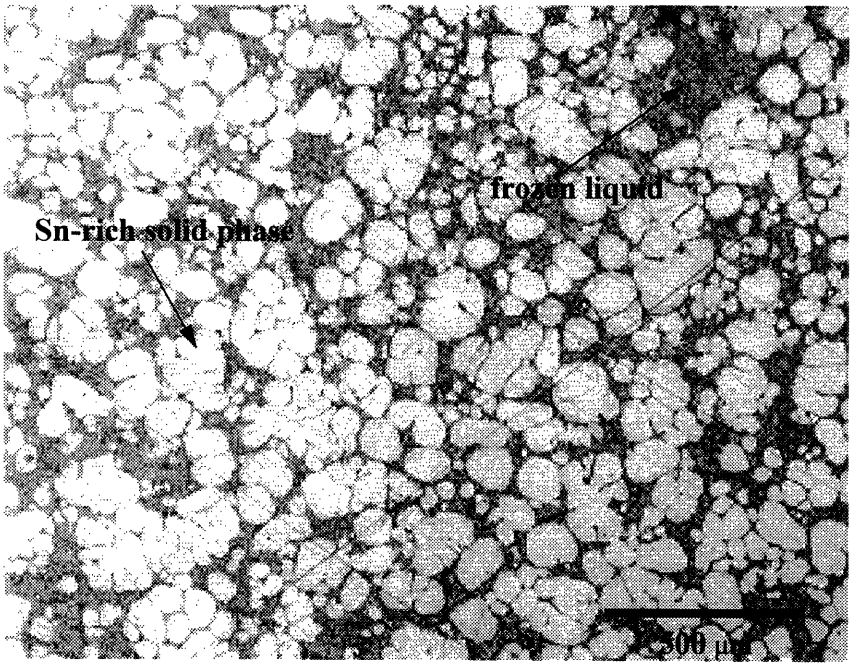

FIGURE 13: Micrograph of semi-solid slurry quenched in ice-water.

4.0 Conclusions

The results of this thesis project was particularly encouraging. We were able to implement a manufacturing concept that can meet an important need for rapid metal component manufacturing.

4.1 Significance of Results

Solid freeform fabrication of fully dense metal components is a significant step in flexible manufacturing. We believe the process presented here has demonstrated a means to overcome hurdles which have remained for some time. To summarize, our process has demonstrated the following key properties:

- Components are metal *and* fully dense. Fully dense metal components have long been a goal of SFF.
- High deposition rates are possible, and components can be fabricated in minutes. All other SFF processes are limited to low deposition rates.
- Component size is virtually unlimited. Present technologies are quite limited in component size.
- Post-processes are not required to sinter, densify, or cure components. Nearly all other SFF processes require a time-intensive post-process.
- Components posses a favorable microstructure. Components have a microstructure more uniform than that found in most castings.

In addition, we have identified some critical process parameters in the successful implementation of this technology. These include:

- Temperature profile and thermal history. The history-dependence of semi-solid alloys and the dependence of solid fraction on temperature makes very precise temperature control essential.

- Flow separation will continue to be a challenge to maintaining a homogeneous stream of semi-solid alloy at a given solid fraction.
- The fraction solid controls the stability of the deposition process due to the tendency for low solid fraction deposits to slump and the tendency for high solid fractions to inadequately bond to previously deposited layers.

4.2 Future Efforts

Certainly much remains to be done to fully implement solid freeform fabrication using semi-solid metals as a production-ready manufacturing process. Several areas of work essential to successful commercialization are outlined here.

First, system models need to be developed. These models are needed to help predict separation of phases during mixing so the phenomena can be prevented and an optimum rotor geometry can be found. In addition, models which could accurately predict solid fraction based on temperature and shear history would be especially useful.

Second, a *fully* continuous system with variable controlled flow rates is desirable. The current Generation II system is a pseudo-continuous system and with a few modifications could made fully continuous. In its current configuration, the deposition rate is a function of gravity, nozzle opening, and solid fraction. Ideally, each of these variables should be decoupled. Generation III was an effort at decoupling these variables, but the Instron we were using was not well suited the amount of loading we imposed. The flow rate should be independently controlled while nozzle aperture size and shape could be changed to aid in the deposition. Efforts are under way to meet these goals.

Third, faster dynamic temperature control would greatly enhance the flexibility of this system. The use of induction heating instead of resistance heaters could allow real-time changes of solid fraction. The advantage of such control is that open cavities could be filled quickly with material of lesser solid fraction after the boundaries of the cavity have been deposited. Induction heaters also present a potential alternative to mechanical stirring.

Fourth, an evolution from this model system to a system using engineering alloys is required. Additional issues of heat transfer and material handling are raised when exploring higher-temperature metals, but conceptually nothing prevents their application. A logical progression may be first to explore aluminum alloy processing while preparing for a transition to ferrous systems.

So, although challenges remain for this process, there has been demonstrated promise. With future efforts, and an application to real engineering alloy systems, SFF using semi-solids should find its home in modern manufacturing.

5.0 References

1. Yoo, J., M.J. Cima, S. Khanuja, E.M. Sachs, "Structural Ceramic Components by 3D Printing," *Solid Freeform Fabrication Proceedings*, The University of Texas at Austin, August 9-11, 1993, pp. 40-50.

2. Carter, W.T. Jr., M.G. Jones, "Direct Laser Sintering of Metals," *Solid Freeform Fabrication Proceedings*, The University of Texas at Austin, August 9-11, 1993, pp. 51-59.

3. Sindel, M., T. Pintat, M. Greul, O. Nyrhila, C. Wilkening, "Direct Laser Sintering of Metals and Metal Melt Infiltration for Near Net Shape Fabrication of Components," *Solid Freeform Fabrication Proceedings*, The University of Texas at Austin, August 8-10, 1994, pp. 94-101.

4. Aubin, R.F., "A world Wide Assessment of Rapid Prototyping Technologies," *Solid Freeform Fabrication Proceedings,* The University of Texas at Austin, August 8-10, 1994, pp. 118-145.

5. Flemings, M.C., "Behavior of Metal Alloys in the Semisolid State," *Metallurgical Transactions A*, May 1991, pp. 957-981.

6. Joly, P.A., "Rheological Properties and Structure of a Semi-Solid Tin-Lead Alloy," Ph.D. Thesis, Department of Metallurgy and Materials Science, Massachusetts Institute of Technology, June 1974.

7. Kumar, P., "Constitutive Modeling and Characterization of the Flow Behavior of Semi-Solid Metal Alloy Slurries," Ph.D. Thesis, Department of Materials Science and Engineering, Massachusetts Institute of Technology, May 1994.

8. Kumar, P., C.L. Martin, S. Brown, "Constitutive Modeling and Characterization of the Flow Behavior of Semi-Solid Metal Alloy Slurries: Part I, The Flow Response," accepted for publication in *Acta Metallurgica et Materialia.*

9. Kumar, P., C.L. Martin, S. Brown, "Constitutive Modeling and Characterization of the Flow Behavior of Semi-Solid Metal Alloy Slurries: Part II, Structural Evolution Under Shear Deformation," accepted for publication in *Acta Metallurgica et Materialia.*

10. Brown, S., P. Kumar, C. Martin, "Constitutive Response of Semi-Solid Slurries," *Proceedings of the TMS Symposium on the Nature and Properties of Semi-Solid Materials,* San Diego, CA, March 1992, pp. 231-244.

11. Kumar, P., C.L. Martin, S. Brown, "Shear Rate Thickening Flow Behavior of Semisolid Slurries," *Metallurgical Transactions A.,* May 1993, pp. 1107-1116.

12. Brown, S.B., M.C. Flemings, "Net-Shape Forming Via Semi-Solid Processing," *Advanced Materials & Processes,* January 1993, pp. 36-40.

13. Brown, S., P. Kumar, C. Martin, "Exploiting and Characterizing the Fundamental Rheology of Semi-Solid Materials," *Proceedings of the Second International Conference on the Semi-Solid Processing of Alloys and Composites,* Massachusetts Institute of Technology, Cambridge, MA, June 1992.

14. Ito, Y., M.C. Flemings, J.A. Cornie, "Rheological Behavior and Microstructure of Al-6.5wt%Si Alloy, *Nature and Properties of Semi-Solid Materials,* J.A. Sekhar and J.A. Dantzig, editors, The Minerals, Metals and Materials Society, 1992, pp. 3-17.

15. Kattamis, T.J., and A.S. Nakhla, "Rheological, Microstructural and Constitutional Study of Semi-Solid Al-4.5%Cu-1.5%Mg Alloy," *Proceedings of the Second International Conference on the Semi-Solid Processing of Alloys and Composites,* Massachusetts Institute of Technology, Cambridge, MA, 1992, pp. 237-249.

16. Nan, W., S. Guangji, Y. Hanguo, "Rheological Study of Partially Solidified Tin-Lead and Aluminum-Zinc Alloys for Stir Casting, *Materials Transactions, JIM,* Vol. 31, 1990, pp. 715-722.

17. Mendez, P., "Joining Metals Using Semi-Solid Slurries," M.S. Thesis, Department of Materials Science and Engineering, Massachusetts Institute of Technology, February, 1995.

18. Nguyen, T.G., M. Suery, D. Favier: "Mechanical Behavior of Semi-Solid Alloys Under Drained Compression with Lateral Pressure," *Proceedings of the Second International Conference on the Semi-Solid Processing of Alloys and Composites,* Massachusetts Institute of Technology, Cambridge, MA, June 1992, pp. 296-305.

19. Hoffman, O., G. Sachs, *Introduction to the Theory of Plasticity for Engineers,* McGraw-Hill Book Company, New York, 1953.

Appendix I: Temperature Histories for Generation I

Below are two representative temperature history curves of Generation I experiments. It is difficult to distinguish the individual curves in these plots. However, one can see the general similarities between the two experiments. In figure I-1, the semi-solid deposition began at time 2900 seconds. Figure 3 provides the temperature profile in the Generation I device at that time. In figure I-2, the flow began at time 3400, at which point the temperature profiles of each experiment matched closely. There are differences in the ramping profiles between the two experiments, but at the time of the actual semi-solid deposition, the temperatures are quite similar.

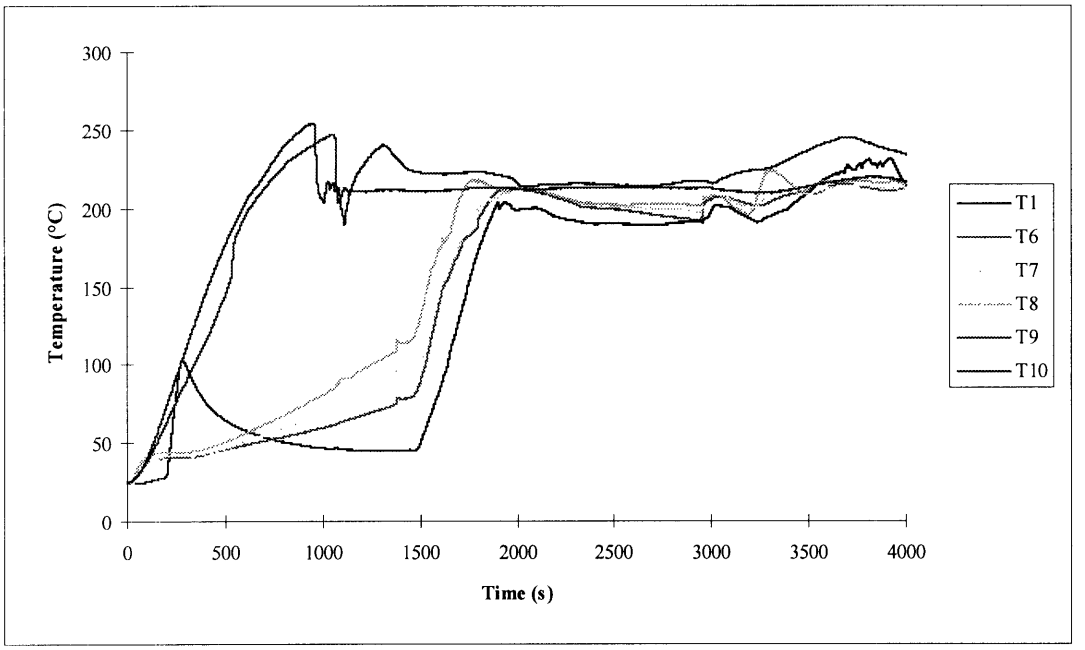

FIGURE I-1: Time-temperature plot of Generation I experiment.

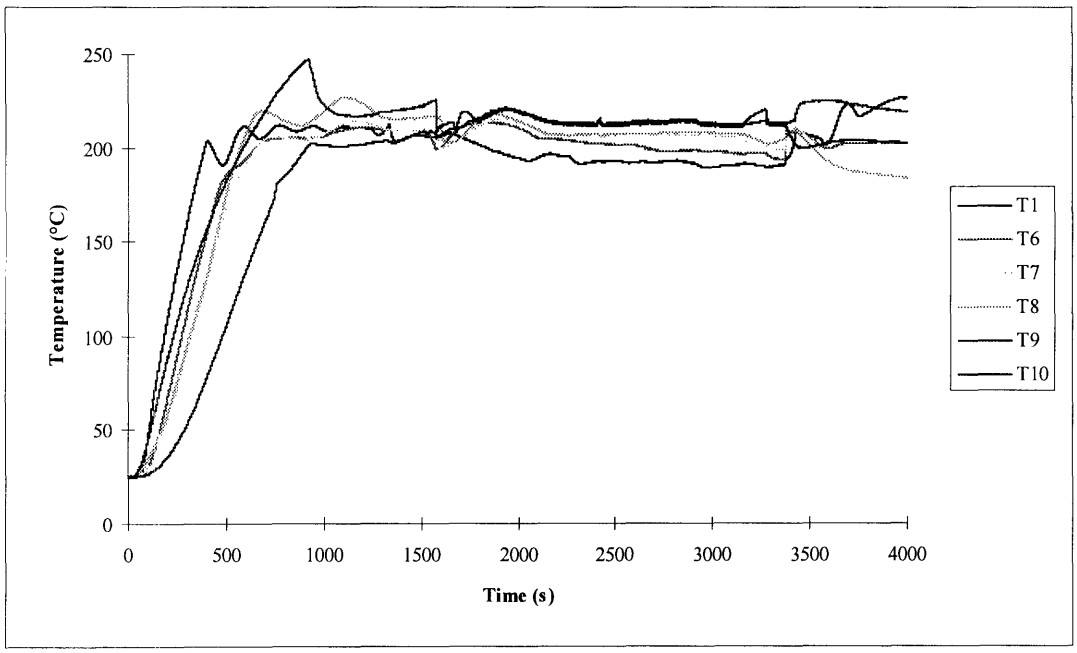

FIGURE I-2: Time-temperature plot of another G-I experiment.

Appendix II: Temperature Histories for Generation II

The following graphs are time-temperature plots for experiments conducted with Generation II. Although it is difficult in the plots to see the individual temperature curves, the plots do show that temperature histories can be repeated. Cooling into the semi-solid regime begins in figure II-1 at approximately 1700 seconds, and in figure II-2 at 1600 seconds. In figure II-1, the semi-solid deposition begins at time 2250 seconds. Figure 5 provides the temperature profile in the apparatus at that time. One can see that the temperatures compare quite closely with those at time 2100 seconds in figure II-2 where the deposition begins.

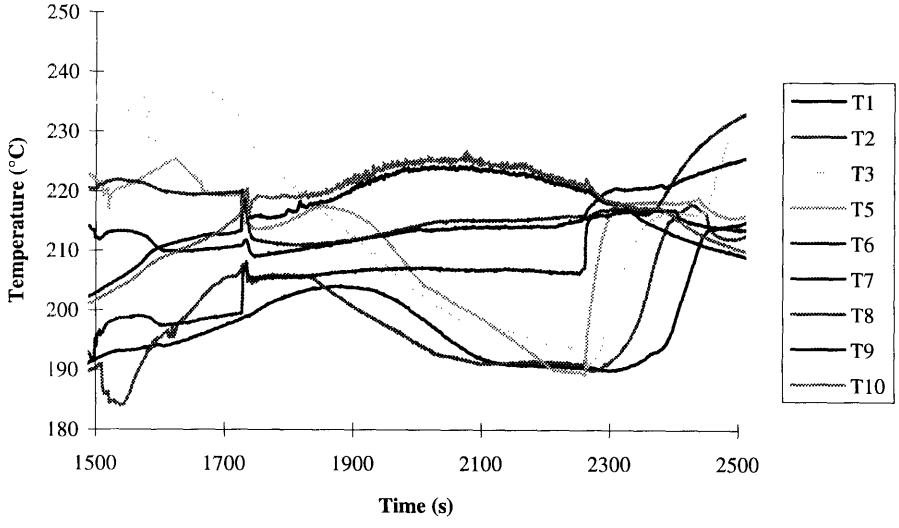

FIGURE II-1: Temperature profile of Generation II experiment.

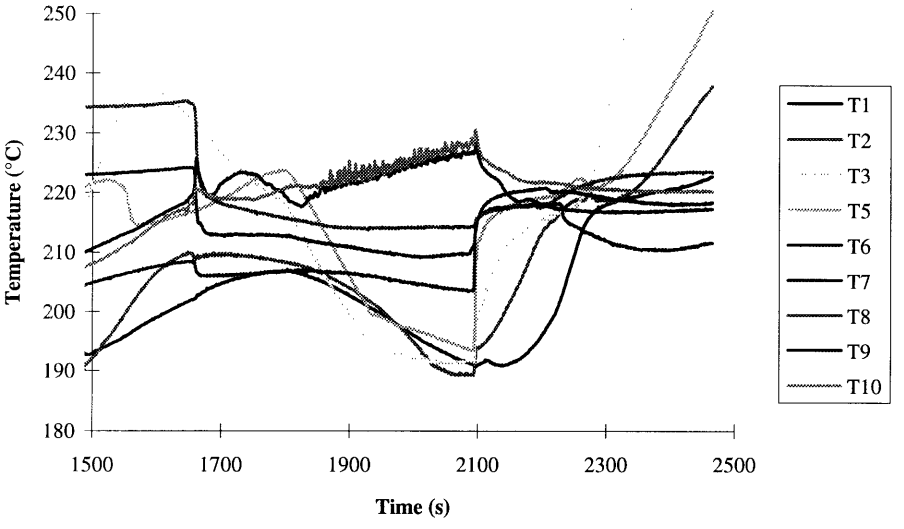

FIGURE II-2: Temperature profile of another G-II experiment.

Appendix III: Machine Photographs

The following figures are photographs of machines presented in this paper. Figure III-1 is a photograph of Generation II. In the center of the photo is the machine itself mounted to a 6 foot tall metal frame. Below the rheocaster is the x-y-z table. It is controlled by the computer to the far right. Above the rheocaster, the Siemens servomotor can be seen. The computer closest to the machine contains the data acquisition software, and also controls the servomotor. To the left is a bank of PID controllers for the various heating elements.

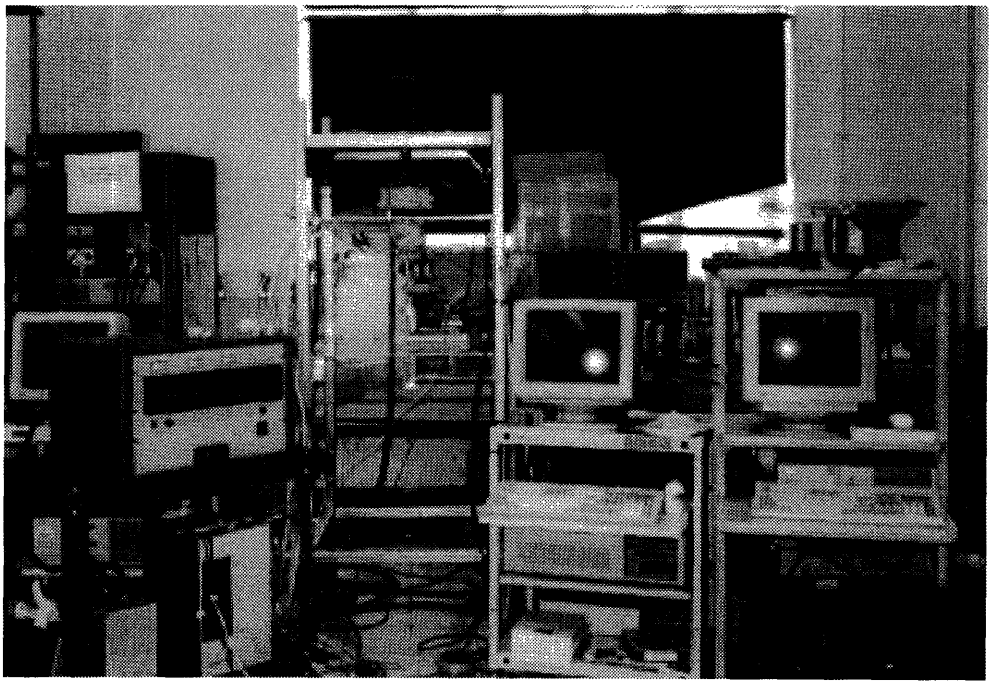

FIGURE III-1: Photograph of Generation II apparatus.

Figure III-2 is a photograph of the Generation III machine. In the photo, the dual screw Instron can be seen housing the axial bearing which holds the shot sleeve, and the load cell with piston. In the foreground rests the computer and data acquisition modules.

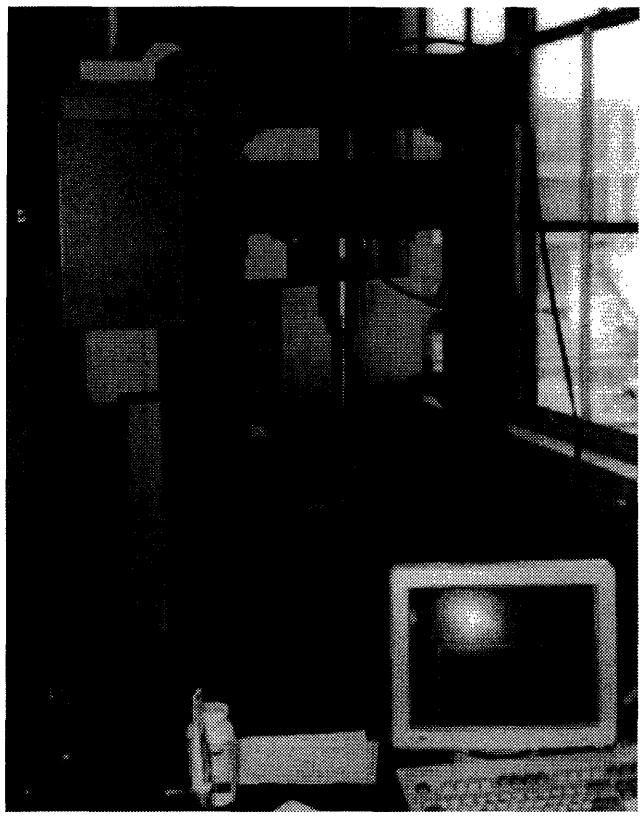

FIGURE III-2: Photograph of Generation III setup.

Appendix IV: Programming Code

This section contains the code written to generate a variety of components with the Motion Architect software. Only the code for the more interesting components is included.

```
***This program creates a pipe bend
def master
comexc1
prun bend
var3=0
t4
while(var3<3000)
 t0.05
 var1=1pm
 var2=2pm
 if(var2<19 and var2>17)
  a,,15
  d,,-3.25
  go,,1
 nif
 var3=var3+1
nwhile
comexc0
end



def bend
drive1111
pscla7874
psclv7874
pscld7874
pa20
pad20
pv20
prtol2

plin45,0

parcm5,5,5
plin0,15.4
parcm-5,5,5
plin-15.4,0
parcm-5,-5,5
plin0,-15.4
parcm5,-5,5

plin13.4,0
parcm7,7,7
plin0,11.4
parcm-7,7,7
plin-11.4,0
parcm-7,-7,7
```

plin0,-11.4
parcm7,-7,7

plin9.4,0
parcm9,9,9
plin0,7.4
parcm-9,9,9
plin-7.4,0
parcm-9,-9,9
plin0,-7.4
parcm9,-9,9

plin5.4,0
parcm11,11,11
plin0,3.4
parcm-11,11,11
plin-3.4,0
parcm-11,-11,11
plin0,-3.4
parcm11,-11,11

plin1.7,0

parcom0,0,0,12.7
plin0.1586,0
parcom0,0,0,12.7
plin0.3722,0
parcom0,0,0,12.7
plin0.5905,0
parcom0,0,0,12.7
plin0.8169,0
parcom0,0,0,12.7
plin1.0,0
parcom0,0,0,12.7
plin1.0,0
parcom0,0,0,12.7
plin1.0,0
parcom0,0,0,12.7
plin1.0,0
parcom0,0,0,12.7
plin1.0,0
parcom0,0,0,12.7
plin0.8169,0
parcom0,0,0,12.7
plin0.5905,0
parcom0,0,0,12.7
plin0.3722,0
parcom0,0,0,12.7
plin0.1586,0
parcom0,0,0,12.7
parcom0,0,0,12.7
parcom0,0,0,12.7

```
parcom0,0,0,12.7


parcop0,-10,0,-5
plin-45,0
end

****This program creates a block
def block
drive1111
indax4
paxes1,2,,3
ppro-.0285
pscla7874
psclv7874
pscld7874
pa20
pad20
pab0
pv20
plin-40,0
var1=8
while(var1>0)
  plin-24,0
  parcom0,-8,0,-4
  plin20,0
  parcop0,-8,0,-4
  plin-20,0
  parcom0,-8,0,-4
  plin24,0
  parcom4,4,0,4
  plin0,16
  parcom-4,4,-4,0
  var1=var1-1
nwhile
parcop0,10,0,5
plin40,0
end

def master
var2=2
while(var2>0)
  prun boxes
  if(var2>1)
     drive111
     indax3
     v30,30,30
     d0,55,12.7
     go1,1,1
  nif
  var2=var2-1
nwhile
drive111
indax3
```

```
v30,30,30
d0,11,-5
go1,1,1
end

***this program creates a set of boxes
def boxes
drive1111
indax4
paxes1,2,,3
ppro-.029
pscla7874
psclv7874
pscld7874
pa20
pad20
pab0
pv20
plin35,0
var1=5
while(var1>0)
  plin12,0
  parcom5,5,0,5
  plin0,12
  parcom-5,5,-5,0
  plin-12,0
  parcom-5,-5,0,-5
  plin0,-12
  if(var1>1)
    parcom5,-5,5,0
  nif
  var1=var1-1
nwhile
parcop-5,-5,-5,0
plin-25,0
end

***this program creates a cylinder
def cylinder
drive1111
indax4
paxes1,2,,3
ppro-.0285
pscla7874
psclv7874
pscld7874
pa20
pad20
pab0
pv20
plin-50,0
var1=20
while(var1>0)
  parcom0,0,0,-20
```

```
  var1=var1-1
nwhile
parcop0,10,0,5
plin50,0
parcop5,-5,0,-5
end

def master
comexc1
prun elbow
var3=0
t7
while(var3<3000)
 t=0.05
 var1=1pm
 var2=2pm
 if(var1<50 and var2<18 and var2>17)
  a,,15
  d,,-3.25
  go,,1
 nif
 var3=var3+1
nwhile
comexc0
end


***This program creates a pipe elbow
def elbow
drive1111
pscla7874
psclv7874
pscld7874
pa20
pad20
pv20
prtol2

;first two lines
plin45,0
parcop0,-3.8,0,-1.9
plin-28.5,0
parcom-1.455,-1.455,0,-1.455
plin0,-1

;first full layer
parcom3,-3,3,0
plin13,0
plin7.15,-.5613
parcom5.6959,1.2595,.7827,9.9693
plin3.5841,2.0218
plin2.22,4.62
plin-2.22,4.62
plin-3.5841,2.0218
```

```
parcom-5.6959,1.2595,-4.9132,-8.7098
plin-7.15,-.5613
plin-13,0
parcom-3,-3,0,-3

;second full layer
plin0,-10.965
parcom3,-3,3,0
plin12,0
plin8.53,-1.02
plin9.02,1.89
parcom0,17.48,-1.8398,8.74
plin-9.02,1.89
plin-8.53,-1.02
plin-12,0
parcom-3,-3,0,-3

;third layer
plin0,-14.49
parcom3,-3,3,0
plin9.2572,0
parcp1.4774,.1097,10
plin7.23,-1.08
plin9.78,0
parcom11.46,11.48,-.9828,12.4411
parcom-11.46,11.48,-12.4428,-.9628
;plin6.36,2.35
;plin3.77,4.11
;plin1.33,5.02
;plin-1.33,5.02
;plin-3.77,4.11
;plin-6.36,2.35
plin-9.78,0
plin-7.23,-1.08
plin-11.2572,0
parcom-3,-3,0,-3

;beginning with 4th layer, circles are
; 2mm smaller radius than before
;fourth layer
plin0,-14.78
parcom3,-3,3,0
plin12,0
plin18.27,-1.62
parcm0,24.04,12.2
plin-18.27,-1.62
plin-12,0
parcom-3,-3,0,-3

;fifth layer
plin0,-14.47
parcom3,-3,3,0
plin11,0
plin13.96,-2.51
```

```
parcom16.01,12.58,2.61,12.58
parcom-16.01,12.58,-13.4,0
plin-13.96,-2.51
plin-11,0
parcom-3,-3,0,-3

;sixth layer
plin0,-12.67
parcom3,-3,3,0
plin11,0
plin10.95,-3.5
plin7.62,-1.59
parcom0,27.38,-2.78,13.69
plin-7.62,-1.59
plin-10.95,-3.5
plin-11,0
parcom-3,-3,0,-3

;seventh layer
plin0,-9.0
parcom3,-3,3,0
plin11,0
plin15.86,-6.96
parcom0,27,0,13.5
;parcom-16.5,13.5,-14.17,0
plin-15.86,-6.96
;shorten to begin taper (was plin-11,0)
plin-8.5,0
parcom-3,-3,0,-3

;eighth layer
plin0,-4.58
parcom3,-3,3,0
;shorten to match above(was plin10.1732,0)
plin7.6732,0
parcop1.5368,-.4235,0,-3
plin15.3915,-8.5841
parcm1,-.4153,3
parcom0,26.9257,-1,13.4629
parcm-1,-.4153,3
plin-15.3915,-8.5841
parcop-1.5368,-.4235,-1.5368,3
;shorten (was plin-10.1732,0)
plin-4.1732,0
parcom-3,-3,0,-3
;plin0,-1
parcom1.04,-1.04,1.04,0

;ninth layer
;shorten to match (was plin15.5395,0)
plin6.3106,0
parcp5.7406,-4.255,6.0

parcom0,8.4969,12.0642,4.0294
```

```
parcp-2.6531,-2.1222,3
plin-4,0
parcm0,-3.519,2
plin4,0
parcp2.6207,-2.1622,3

;tenth layer
;parcom0,8.4969,12.5238,4.255
parcom0,8.4969,12.5238,4.255
parcp-2.6531,-2.1222,3
parcm0,-3.519,2
parcp2.6207,-2.1622,3

; eleventh, twelfth layers
parcom0,0,12.0642,4.0294
parcom0,0,12.0642,4.0294

;leave component
plin0,-20
parcop-5,-5,-5,0
plin-30,0

end


***this program creates an egg
def master
comexc1
prun egg
var3=0
while(var3<3000)
 t=0.05
 var1=1pm
 var2=2pm
 if(var1<50 and var2<3.5 and var2>2.5 and var3>100)
  a,,15
  d,,-3.25
  go,,1
 nif
 var3=var3+1
nwhile
comexc0
end

def egg
drive1111
pscla7874
psclv7874
pscld7874
pa20
pad20
pab0
pv20
plin45,0
```

```
parcom0,30,0,15
parcm-2,-29.8661,15
plin4,-2.0159
parcom-4,0,-2,16.8819
plin4,-1.5096
parcom-4,0,-2,18.3916
plin4,-1.0056
parcom-4,0,-2,19.3972
plin4,-.5026
parcom-4,0,-2,19.8997
plin4,-.2010
parcom-4,0,-2,20.1007

parcom0,0,2,20.1007

plin4,.2010
parcom-4,0,-2,19.8997
plin4,.5026
parcom-4,0,-2,19.3972
plin4,.9050
parcom-4,0,-2,18.4922
plin4,1.1068
parcom-4,0,-2,17.3853
plin4,1.3093
parcom-4,0,-2,16.0761
plin4,1.7147

prtol2
parcom-4.7647,.1274,-2,14.3614

parcm1.3869,.2345,2
plin3.0737,1.7877
parcp.625,.2346,2
parcom-5.2305,.1292,-2.3209,11.9772
parcm1.6094,.2938,2
plin2.9908,2.0546
parcp.6415,.2903
parcom-4.3321,-.0778,-2.3321,9.2093


parcom30,30,0,30
plin0,80


end
```